Role of Co antisite segregation in the CoAl(111) surface

L. Hammer, V. Blum,* Ch. Schmidt, O. Wieckhorst, W. Meier, S. Müller, and K. Heinz
Lehrstuhl für Festkörperphysik, Universität Erlangen-Nürnberg, Staudtstr. 7, D-91058 Erlangen, Germany
(Received 24 August 2004; published 22 February 2005)

The geometrical and chemical structure of the CoAl(111) surface is investigated by quantitative low-energy electron diffraction and calculations applying density functional theory. The stacking sequence of the top four atomic planes is Al-Co-Co-Co, followed below by the usual alternating B2 stacking. The topmost layers thus form a unit cell of the well-known bcc-based $D0_3$ crystal structure [the A_3B superlattice of bcc(111) atomic planes], although the bulk phase diagram of CoAl shows no $D0_3$ phase. Its occurrence and stability at the surface is due to a slight Co excess of the nominally stoichiometric sample, equivalent to the presence of Co antisite defects in the bulk. These defects are enriched in undercoordinated near-surface sites of the Al sublattice, which lowers the total energy because more Al atoms can then reside in fully coordinated bulk Al sites. However, all three topmost layers are undercoordinated, and the segregation of Co antisite defects competes with a general trend towards a termination of the surface by Al. In the balance, the third layer is the preferred plane for Co antisite defects.

DOI: 10.1103/PhysRevB.71.075413 PACS number(s): 61.14.Hg, 64.75.+g, 68.35.Dv, 68.35.−p

I. INTRODUCTION

Intermetallic phases have been a subject of research for almost a century,[1] and the idea that atomic ordering is responsible for their wide spectrum of properties is almost as old.[2] Their order properties in the three-dimensional bulk became accessible by x-ray diffraction, but due to the initial experimental challenges of surface science, studies of their boundaries—their surfaces—have a much younger history.[3] In a single bulk intermetallic phase, the distribution of the elements is usually locally homogeneous, but in a surface this need not be the case. Instead, individual components may be enriched at a surface or grain boundary, and the importance of this *segregation* for, e.g., mechanical or corrosion properties of a material has long been recognized.[4] Segregation is a well-studied phenomenon in weakly ordering or even disordered systems.[5] Yet, it came as a recent surprise that the surface composition of strongly ordering compounds is also not necessarily a property of the ideally stoichiometric bulk.[6,7] Instead, the atomic concentration and order of a surface may be determined by the material's intrinsic defects, which are due to minor compositional deviations. For the (100) surface of the B2-ordered compound CoAl[6] and for the (111) oriented surface of the $L1_0$ compound NiPt,[7] it was shown that the composition of the outermost atomic plane depends on the sign of the stoichiometric deviation of the underlying bulk from the ideal ordered phase.

Both CoAl(100) and NiPt(111) are relatively close-packed surfaces, where the impact of bulk defects stays mostly constrained to the topmost atomic layer. In the present work, we investigate the much more open (111) oriented surface of CoAl, and obtain the paradoxical result that its intrinsic defects (Co antisite defects on the Al sublattice of the crystal) influence not the topmost layer, but rather a deeper one (the third). Our experimental conclusion is derived from investigations by quantitative low-energy electron diffraction (LEED) and Auger electron spectroscopy (AES), and is fully confirmed by density functional theory (DFT) studies of the detailed geometric and energetic properties of different possible surface terminations. In our study, we encounter the rather rare situation that quantitative LEED, based on the quality of the fit between calculated model spectra and experimental data, cannot differentiate between two very different surface models. Here, one may erroneously mask the presence of intrinsic Co antisite defects by constructing an alternative, mixed-domain termination model of the bulk-ordered system, very similar to a seminal[8–10] and highly controversial[11–13] proposal for the related system NiAl(111). At the time of the NiAl(111) debate, the key role of constitutional defects for surfaces was unknown. In our present study of CoAl(111), the powerful combination of quantitative diffraction analysis with fully *ab initio* model calculations resolves the conflict unequivocally in favor of Co antisite defects. In addition, DFT also provides surface structural parameters of phases which were not accessed in the work presented in this paper.

We place our work in the broader context of transition-metal aluminide surface physics in the following section, and then address the properties of CoAl(111) in AES, quantitative LEED, and DFT studies of surface geometry and energetics.

II. SEGREGATION IN 3D TRANSITION-METAL ALUMINIDE SURFACES

The *3d* transition-metal aluminides Ni-Al, Co-Al, and Fe-Al should appear strikingly similar as they each form intermetallic compounds of the B2 type around 1:1 stoichiometry. They are of particular technological interest for high-temperature applications due to their low density and good corrosion resistance. In the following, we summarize the properties of their surfaces in earlier studies (for earlier reviews see also Refs. 14 and 15), and highlight the role of CoAl(111) to advance this understanding.

 ©2005 The American Physical Society

Ni-Al: Early investigations of nominally stoichiometric and ordered NiAl surfaces by quantitative LEED checked only for the geometry and the chemical termination of the surfaces without considering the possibility of segregation. For (100) and (111) surfaces with their chemically alternating layers, these studies suggest a single-domain Al termination for (100),[16,17] but surprisingly the *coexistence* of Al- and Ni-terminated domains for (111) orientation.[8–10] Subsequent investigations using low-energy ion scattering (LEIS) and scanning tunneling microscopy (STM) found a reduced Al concentration in the top layer of the (100) surface.[18–21] The Al deficiency was attributed to the presence of either Ni antisite atoms or vacancies, and was shown to depend on the surface preparation procedure. Even a pure Ni termination is reported for high-temperature flash-annealed NiAl(100) surfaces with and without vacancies as determined by x-ray diffraction (XRD)[22] and LEIS.[19] Doubts regarding the mixed termination of the (111) surface were also raised,[11–13] and a full consensus on its verity was never reached. In contrast, no controversies exist for the NiAl(110) surface, which shows no segregation. All lattice planes are of the same bulklike mixed stoichiometry, and a chemically induced rippling was found for the outermost layer.[18,23–28]

Fe-Al: For Fe-Al surfaces, much recent work has focused on the geometrical and chemical structure of the (100) orientation for various Fe-rich $Fe_{1-x}Al_x$ samples in the range $0<x\leqslant 0.5$ (i.e., including FeAl). For all compositions, Al segregates to the surface, and the top layer consists almost completely of Al for $x=0.30$ and higher.[29,30] For all stoichiometries, the order of the subsurface region is determined by the phase diagram. In the same way, the local stoichiometry of the subsurface region also determines the transitional order of a sputtered, and therefore Al-depleted, surface on its way back to equilibrium during annealing.[29,31] No bulk terminated surface is observed for the FeAl(110) surface. Instead, its equilibrium phase is reconstructed to accommodate Al segregation by way of an incommensurate surface layer of $FeAl_2$ stoichiometry.[32–35] The FeAl(111) surface shows even more extreme behavior. Al segregation shows no saturation with increasing annealing temperature and the surface exhibits strong reconstructions. A $(\sqrt{3}\times\sqrt{3})$ phase is presumably characteristic for a Fe_3Al-like bulk,[36] and a (3×3) superstructure forms on FeAl when annealing in a temperature range above 1000 K.[34] The situation is similar for the (210) surface, while the (310) surface is even unstable and develops lower-index facets.[34]

Co-Al: To our knowledge there are only two quantitative investigations of surface geometry and chemistry. Quantitative LEED revealed that CoAl(110) is bulk terminated just as NiAl(110), with a similar rippling of the first layer.[37] Yet, about 20% of the Al sublattice sites of the second layer are occupied by Co. In a combined LEED and DFT study, Co antisites were also found in the CoAl(100) surface,[6] and additional Co antisites accumulate in the third layer for yet larger off-stoichiometries of the underlying bulk.[38] The antisites concentrate particularly in the top layer which, according to the chemical sequence of the following layers, should consist purely of Al.

Mechanism: The various findings were qualitatively explained by the competition between a tendency towards Al surface segregation and opposing forces favoring chemical ordering.[6] On the one hand, the surface energy of (hypothetical) bcc Al is much lower than the values of bcc Fe, Co, or Ni: In the case of the (100) surface the energies are 0.623 eV/atom for Al, but 1.150, 1.175, and 1.038 eV/atom for Fe, Co, and Ni, respectively.[39] Al surface segregation in FeAl can be attributed to the reduction of the surface energy. On the other hand, the energy gain for chemical ordering would seem to enforce strict order in the entire crystal including the surface. The preference for order may be estimated by the modulus of the alloy formation enthalpy from elemental crystals, which is much larger for NiAl (0.64 eV/atom)[40] or CoAl (0.55 meV/atom)[41] than for FeAl (0.26 eV/atom).[41] So, no pronounced aluminum segregation beyond a bulklike termination is observed in NiAl, unlike in FeAl.

In CoAl, the situation should be similar to NiAl because of the similar energetics involved. However, an accumulation[6,37] and even lateral ordering[38] of Co antisite defects at CoAl surfaces was observed in all investigations up to the present one. In view of the large energy required to create a Co antisite (1.29 eV),[42] it was argued[6] that a Co excess must already exist in the (evidently) slightly off-stoichiometric bulk: Co antisites are the dominant defect type on the Co-rich side of the phase diagram.[42–45] Their segregation is favorable *because* of the strong ordering tendency (large modulus of the alloy formation enthalpy) in the bulk. The atomic coordination of surface sites is reduced, making these an obvious location to reduce unfavorable bonding. Still, there is competition with the overall trend of Al segregation. In the balance, transition-metal defect segregation yields 0.85 (0.61)eV in the (100) surface of CoAl (NiAl), indeed favoring antisite segregation. On the other hand, it would *cost* 0.05 eV in FeAl,[6] and consequently is not observed even for an Fe-rich bulk. Finally, this interpretation may also account for the varying reports regarding the existence of surface Ni antisites in NiAl(100).[18,20,21] Even minor variations of the off-stoichiometries in the samples investigated in these studies may lead to completely different segregation profiles.

The present paper's investigation of the geometrical and chemical structure of the CoAl(111) surface adds to the catalogue of surface structures, and is a crucial test for the above outlined picture of surface segregation. According to that, CoAl with its large formation enthalpy should be more similar to NiAl than to FeAl. So, it will be interesting to see whether or not CoAl(111) reconstructs [as does FeAl(111) in contrast to NiAl(111)] and whether Al segregation as in FeAl, or antisite segregation as in the (100) and (110) orientation of CoAl [and in NiAl(100)] occurs. Furthermore, CoAl(111) planes are rather open (see Fig. 1), with an accordingly short interlayer distance. The topmost *three* surface planes lack crystallographic nearest (nn) and next nearest neighbors (nnn). Atoms in layers one, two, and three have only four nn (three nnn), seven nn (three nnn), and seven nn (six nnn), respectively. Only fourth and deeper layer atoms are provided with all their eight nn and six nnn. This leads to an interesting near-surface bonding environment, and it is not clear which layer(s) would be affected by a possible deviation from bulk-like B2 ordering.

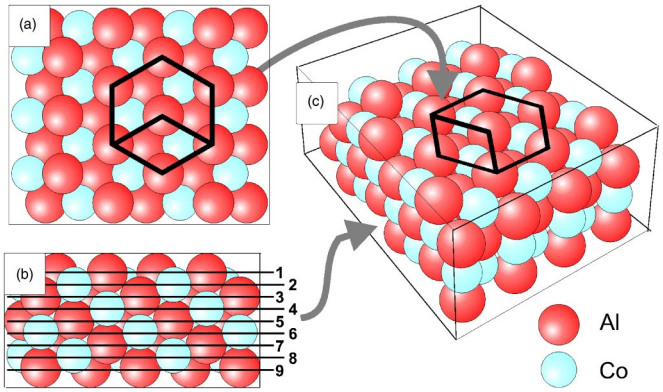

FIG. 1. (Color online) Ball model of an Al-terminated CoAl(111) surface in (a) top, (b) side, and (c) perspective view.

III. EXPERIMENTAL AND COMPUTATIONAL DETAILS

The experiments were performed with the sample in a standard UHV vessel. During the experiments, the pressure (base value: 8×10^{-11} hPa) did not rise beyond 4×10^{-10} hPa. The vessel was equipped with a four-grid back-view LEED optics which also served as a retarding-field analyzer for AES. Additionally, an ion sputtering source and a quadrupole mass spectrometer were available. The sample, which was oriented with an accuracy of ±0.5°, could be cooled to about 90 K by contact with a liquid nitrogen reservoir and heated up to 1450 K by electron bombardment. The temperature was measured using a NiCr-Ni thermoelement. After *ex situ* polishing, the sample was fully cleaned *in situ* by repeated Ne^+ ion sputtering and annealing at about 1350 K until impurities were no longer detectable in the Auger spectrum.

In order to minimize residual gas adsorption, maximum speed for the LEED measurement was realized by video-taping diffraction patterns in their entirety. The measurements were done at normal incidence of the primary beam and for energies between 25 and 500 eV, in steps of 0.5 eV. The computer controlled off-line evaluation, including background subtraction,[46] yielded the intensity versus energy, $I(E)$, spectra of 14 (integer order) symmetrically inequivalent diffraction spots. The resulting cumulative data-base width amounts to $\Delta E=3020$ eV. The AES data were recorded in the derivative mode, whereby the peak-to-peak signals of Co and Al, I_{Co} and I_{Al}, were taken for the Co(*MVV*) and Al(*LVV*) transitions at 53 and 68 eV, respectively. Some overlap of these lines was corrected using reference samples of known composition. The ratio of the two signals, $r_{Al/Co}=I_{Al}/I_{Co}$, was taken to monitor the development of the surface composition during annealing.

The quantitative LEED intensity analysis was performed using the perturbation method Tensor LEED[47,48] through the Erlangen program package TensErLEED.[49] This includes chemical Tensor LEED[50,51] which allows the easy (perturbative) substitution of an Al atom by a Co atom (and vice versa). For the full dynamic reference calculation, a plane-wave based layer stacking scheme could not be used because of the small interlayer spacing in the (111) surface (bulk value 0.826 Å). Instead, the entire surface volume penetrated by the electrons had to be treated as a single slab in angular momentum space, requiring as many as 18 layers for satisfactory convergence. Up to 11 relativistic and spin-averaged phase shifts proved sufficient to describe the atomic scattering up to 500 eV. The different scattering strength and angular characteristics of Co and Al allow one to distinguish the two elements in the analysis. The nonstructural parameters of the bulk were represented by the same values which had proved to be successful in the analysis of CoAl(110)[37] and CoAl(100).[30] The real part of the inner potential was energy dependent, $V_{0r}=V_{00}+E/150$, with V_{00} adjusted in the course of the structural search. The imaginary part was set to $V_{0i}=5.5$ eV, the lattice parameter was $a=2.86$ Å, and the vibrational amplitude for bulk atoms was $u^b=u^b_{Al}=u^b_{Co}=0.09$ Å (which agrees with the room temperature value[52] extrapolated to 90 K). By means of thermal Tensor LEED[53] element-independent vibrational amplitudes u_i $(i=1,2,3)$ for the top three layers were determined in the structural search. The search was carried out using a frustrated simulated annealing procedure,[54] and was guided by the Pendry R factor[55] for the quantitative comparison of experimental and computed spectra. Statistical error limits for all optimized parameters were subsequently estimated by way of the variance of the R factor, $var(R)=R_{min}\sqrt{8V_{oi}/\Delta E}$.[55] The Pendry R factor was also used to compare experimental $I(E)$ spectra for different conditions, and, in particular, to quantify their change during annealing.

The *ab initio* calculations employed spin-polarized DFT in the generalized gradient approximation (GGA).[56] Ultrasoft pseudopotentials for Co and Al allowed for the fast solution of the Kohn-Sham equations by means of the VASP computer code.[57] Test calculations produced formation enthalpies of bulk CoAl, FeAl, and NiAl which deviate no more than 40 meV from the experimental values given in Sec. II. The bulk lattice parameters of these alloys could be reproduced within about 0.01 Å [CoAl: 2.855 Å (DFT) vs 2.862 Å(exp)]. The surface was simulated by a periodic arrangement of symmetric slabs of 19 atomic layers (Co or Al), which were separated by vacuum slabs equivalent to a thickness of 17 layers. The plane-wave basis was defined by a cutoff energy of 300 eV and an $18\times18\times2$ *k*-point mesh in the irreducible Brillouin zone.

IV. THE ANNEALING PROCESS MONITORED BY AES AND LEED

Through preferential sputtering of Al, the initial surface cleaning procedure leaves behind a surface slab which is somewhat enriched in Co. In order to provide a well-defined starting point for the experiments, the sputter-cleaned sample was subjected to a short flash to about 1370 K (to remove any possibly adsorbed residual gas), a subsequent quench to about 90 K, and further sputtering for 30 min ($p_{Ne}=5\times10^{-5}$ hPa, U=1 kV, $j\approx4\ \mu A/cm^2$). By preferential sputtering this creates an Al-depleted surface slab of about 43% Al (estimated from the Auger signal), in good agreement with the literature.[58] From here, the sample was annealed in steps of increasing temperature, marking the surface's way back into equilibrium with the deeper-lying bulk. This can be

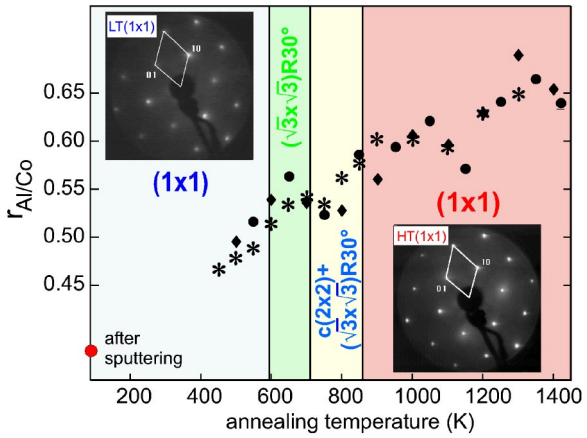

FIG. 2. (Color online) Development of the Auger ratio $r_{Al/Co}$ with annealing temperature. Each curve begins with the sample sputtered at 90 K. Symbols + and × refer to step-wise annealing (5 min at each step) of increasing temperature. Symbols ⋆ stem from the same stepwise procedure, but with the sample resputtered after every three annealing steps. Low and high temperature (1 ×1) LEED patterns are given as insets.

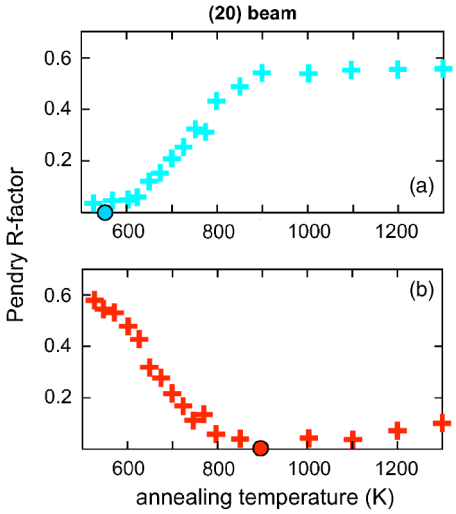

FIG. 3. (Color online) Development of the Pendry R factor for intensity spectra of the (20) beam as function of the annealing temperature with the phase annealed at 550 K as reference in (a) and the phase annealed at 900 K as reference in (b). The reference temperatures are indicated by full circles in each case.

followed by AES as well as by LEED, in the latter case both by the appearance of the diffraction pattern and the development of beam intensity spectra. Each annealing step lasted for about 5 min at a constant temperature, after which the sample was quenched to 90 K in order to obtain AES and LEED data. The procedure was varied by either continuing the anneal immediately, or by resputtering the surface after every third step. The final annealing temperature could not exceed 1400 K, since evaporation of Al starts here as indicated by the mass spectrometer.

Figure 2 displays the development of the ratio $r_{Al/Co}$ during step-wise annealing. Three independent annealing experiments lead to rather similar curves of $r_{Al/Co}$ versus the annealing temperature. Evidently, $r_{Al/Co}$ is characteristic for the respective annealing temperature. However, it does not describe stoichiometric equilibrium with the bulk as another experiment shows: Returning to a lower temperature does not reproduce the former Auger ratio. Apparently, in the surface slab probed by the Auger electrons the Al concentration grows steadily in a diffusion limited process without, however, reaching a saturation level characteristic for the equilibrium state of the fully recovered bulk composition. For low (⩽600 K) and high (⩾820 K) annealing temperatures (1×1)-symmetric LEED patterns develop as inserted in Fig. 2. The low annealing-temperature phase, LT(1×1), is not as well ordered as the high annealing-temperature phase, HT(1×1), as obvious from the background level and from the strength and width of the diffraction spots. In addition, the range where two superstructures develop is also indicated in Fig. 2. The extra spots of both are very weak, i.e., either the corresponding structural deviations from (1×1) order are similarly weak, or the respective phases develop in long-range order only on small patches of the surface. Therefore, we do not address these phases any further.

The development of LEED beam intensities as a function of annealing temperature is an indicator for the corresponding change of surface structure. We find that spectra change gradually with annealing temperature, whereby the main peaks remain similar throughout but intermediate spectral features are modified considerably. These changes can be mirrored quantitatively by the behavior of the Pendry R factor between one spectrum at a fixed annealing temperature ("reference" spectrum) and the spectra at all other values. This development is displayed in Figs. 3(a) and 3(b) using the spectra of the (20) beam which prove to be most sensitive. In panel (a) the fixed spectrum corresponds to the LT(1×1) phase annealed at 550 K (full circle). At about 620 K the spectra start to deviate from the reference whereby the changes saturate above 850 K. As the Pendry R factor is no metric measure, this behavior needs to be verified with the high-temperature phase as reference (900 K). The result is displayed in Fig. 3(b). Indeed, all changes occur in the temperature range below 850 K. So, the LT(1×1) and HT(1×1) phases must correspond to different structures. The fact that there are only very minor changes within the corresponding (1×1) phases, in spite of the steadily increasing Auger ratio $r_{Al/Co}$, deserves more discussion. We shall address this point after the following description of the LEED structure analysis.

V. LEED STRUCTURE ANALYSIS OF THE HT(1×1) PHASE

As the LT(1×1) phase appears to be of only limited order, we concentrate on the quantitative LEED intensity analysis of the HT(1×1) phase in the following. $I(E)$ spectra for this phase were taken at 90 K from samples annealed at 900 and 1300 K. The beam averaged R factor between both sets is as small as R=0.058. This indicates that the respective structures must be very similar, wherefore it is sufficient to analyze only one of them. We chose the 1300 K data set.

Guided by earlier investigations of aluminide surfaces, we allowed for two different types of models. First, early LEED studies devoted to NiAl surfaces claim ordered bulklike terminations,[8–10] with the interesting finding of a domain mix with both bulklike terminations present at the surface. We call this class of models the "MT model." Second, our recent analysis of CoAl(100)[6] revealed a unique and overall bulklike layer stacking sequence, but with significant site-dependent deviations from ideal stoichiometry in very specific surface sites (Co antisite defects). This class of models will be called the "$AlCo_3$ model," for reasons which will become obvious below.

MT model: As the bulk of CoAl is of B2 structure, it is reasonable to test surface models in which this structure extends up to the vacuum. The B2 structure is an alternating superlattice of (111) Al and Co atomic planes, allowing two possible terminations—Al or Co. For each, we varied up to eight interlayer spacings and the vibrational amplitudes of the top three layers, i.e., eleven parameters. However, the best-fit R factor of the B2 structure is unsatisfactory for both terminations ($R_{B2}^{Co} > R_{B2}^{Al} = 0.252$). This situation is similar to that reported in the LEED analysis of NiAl(111), and our next step was to try an equivalent mixed-domain termination model here (MT model). In the resulting structural search, one must now allow for layer relaxations and atomic vibrations to vary *independently* in both domains. This more than doubles the number of adjustable parameters (2×11 + domain weight = 23 parameters). As a consequence, the fit *must* improve simply due to the sheer number of free parameters. Still, the best-fit R factor now amounts to $R_{B2}^{Al+Co} = 0.174$ with 70% (30%) of the surface terminated by Al (Co). This improvement is significantly larger than the R factor variance [$var(R) = 0.021$] and can therefore not be directly dismissed as an artifact of too many free parameters. Some further insight can be derived by inspecting the structural parameters associated with this best fit. In particular, it turns out that the interlayer spacing between first and second layer in the Co-terminated domain, d_{12}^{Co}, is contracted by more than 40%, a rather unusual amount. The distance of the top layer atoms' nearest neighbors, $d_{14}^{Co} = 2.44$ Å, is kept reasonable (bulk value 2.48 Å) because of expanded d_{23}^{Co} and d_{34}^{Co}, but the nearest neighbor distance $d_{47}^{Co} = 2.13$ Å is physically unacceptable. This raises considerable doubt concerning the validity of the MT model as such. [Interestingly, a similarly disturbing value of d_{12} was also found for the Ni-terminated domain in the analysis of NiAl(111), but was not further commented.[17]] Additionally, preliminary STM investigations on the same sample[59] revealed only double steps (and multiples of those), except where bulk antiphase domain boundaries cross the surface plane. This points to a single type of termination.

$AlCo_3$ model: Returning to single-domain terminations, we allowed for deviations from the B2-stacking as a new degree of freedom. As atoms in the top three (111) layers are undercoordinated, surface-related effects may affect all of them and even deeper layers can be modified as a consequence. To capture all conceivable terminations, we allowed for chemically pure but different layers in a surface slab of eight layers, with B2-stacking order below (starting either with a Co or an Al layer)—a total of $2 \times 2^8 = 512$ inequivalent stacking sequences. Even with only one full-dynamic reference calculation per stacking sequence, and all subsequent variation of geometric and vibrational parameters handled by Tensor LEED, 512 different stacking sequences would still amount to a near-impossible computational task. We therefore chose to involve *chemical* Tensor LEED as well. To be as neutral as possible, two reference calculations were performed with the top eight layers occupied by $Al_{50}Co_{50}$ (the average scattering matrix of Co and Al according to the average *t*-matrix approximation).[60] The stacking sequence was then determined by allowing either Co or Al to occupy each site, naturally with different geometric and vibrational parameters as outlined above.

In the following structural search, we found that a special stacking sequence of chemically pure layers is favored over all others, including both bulklike terminations. The sequence (from top) Al-Co-Co-Co-Al-Co-Al-Co… produces a fit with $R^{AlCo_3} = 0.195$. This value is lower than that of any other single termination by clearly more than the R-factor variance (=0.024). The aforementioned bulklike Al-terminated stacking sequence comes in second place; it only differs from the improved model in the third atomic layer, where Al atoms are replaced by Co. In fact, this $AlCo_3$ layer sequence at the very surface is also the defining element of the well-known bcc based $D0_3$ structure—the A_3B superlattice of (111) planes. If correct, a unit cell of this structure is stabilized at the CoAl(111) surface, although no corresponding phase exists in the bulk phase diagram of Co-Al. We also point out that the $AlCo_3$ element exists only at the surface: All models which extend this stacking deeper into the surface must be discarded because of considerably higher R factors involved ($R > 0.26$).

The full best fit of the $AlCo_3$ model still exhibits one seemingly counterintuitive feature: The vibrational amplitude of atoms in the third layer is higher than in the second one (0.16 Å vs 0.14 Å). This behavior could be a consequence of some actual substitutional disorder in the third layer, reflecting the well known coupling between this disorder and vibrations.[61] We were therefore tempted to allow for some substitutional disorder in a follow-up step. Taken strictly seriously, one would have to introduce an elemental concentration parameter for each layer, including element-specific positions in each layer due to the different chemical coordination towards atoms of adjacent layers (Tensor LEED can model this effect even in the case of disorder).[37] In total, the number of free parameters in the structural search would be almost tripled, and not surprisingly, a straightforward fit attempt produces no convergence of the search. In order to obtain a good approximation to our hypothesis of disorder near the surface, we tested it in the top three layers only, and included element-specific positions in only the third layer (which showed the unusual vibrational amplitude). This structural search converges quickly, reaching an optimum R-factor $R = 0.172$ with reasonable vibrational amplitudes 0.20, 0.12, 0.12 Å in layers 1-3, respectively, versus 0.09 Å fixed for bulk layers. While the top layer still consists purely of Al, the best-fit indicates 15% and 30% Al in layers 2 and 3, respectively. A coupling between vibrations and chemical degrees of freedom is clearly a consistent explanation for the

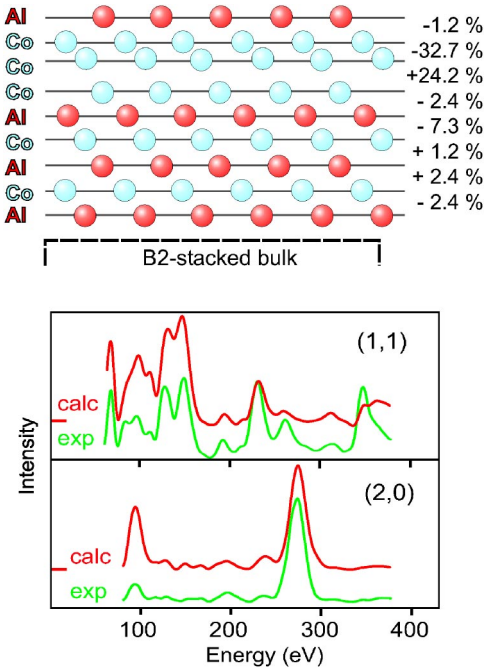

FIG. 4. (Color online) Top: $AlCo_3$ model in side view. On the left the resulting atomic layer stacking is given whilst the percentages on the right stand for the relaxations of the layer spacings relative to the bulk value (d_b=0.826 Å). Bottom: Comparison of experimental and best-fit calculated spectra of the $AlCo_3$ model for two selected beams.

vibrations found in the ordered $AlCo_3$ model. On the other hand, the reduction of the R factor amounts almost precisely to the R-factor variance (0.024), i.e., the actual degree of substitutional disorder found is not well outside the limits of statistical errors. In order to avoid the impression of an overly accurate determination of these parameters, we limit our discussion to the ordered $AlCo_3$ model in the following, keeping in mind both the possibility for some substitutional disorder and the fact that the resulting fit is fully consistent with the conclusions highlighted below.

The ball model of the ordered $AlCo_3$ model is given in the top panel of Fig. 4, together with the percentages of layer relaxations. For visual comparison, experimental and best-fit calculated spectra are displayed below for two selected beams. The complete set of the resulting best-fit parameters is displayed in Table I (see Sec. VI) including the error limits as estimated by the variance of the R factor with, however, no parameter correlations considered (as usual). As stated above, the crystal is capped by a pure Al layer followed by three layers consisting of Co. In view of the remaining B2-like stacking sequence, the Co atoms in the third layer reside on the nominal Al sublattice of the crystal, and therefore constitute antisite defects—similar to those found in our earlier investigations of CoAl(100)[6] and CoAl(110)[37] (with both samples annealed at about 1000 °C). However, these antisites reside in the third layer for CoAl(111), and not in the first as for CoAl(100). We will show quantitatively below how this result is consistent with the general competition between antisite defect segregation on one hand, and an Al surface termination on the other.

We know of no other example of the unusual layer stacking exhibited by CoAl(111). Therefore, we postpone the discussion of the structural details found in the LEED analysis to the next section, in which the structure of CoAl(111) is calculated by DFT, both for the $AlCo_3$ surface stacking and for ordinary B2 stacking. However, at least two additional points deserve attention. The first concerns the Al content of the surface, which increases continuously with increasing annealing temperature according to Fig. 2, and shows no saturation. As previously noted, the phase reached by a certain annealing temperature is not an equilibrium state for which this temperature were characteristic (reduction of the temperature fails to reestablish the reduced Auger ratio). Rather, the actual stoichiometry in the surface slab is established in a diffusion limited process. The observed continued increase of the surface Al content is well consistent with the limited resolution of actual chemical disorder in the $I(E)$ analysis. Of course, an equivalent argument holds also for the LT(1×1) phase. A test run for the LT(1×1) phase indicates that the Al concentration in the first three layers is similar to the HT(1×1) phase, but is lower in deeper layers. This indicates that the processes to establish the Al termination and the antisite occupation of the third layer are rather fast, in contrast to the restoration of the B2-stacking below.

The second point to discuss is the fact that, within the variance of the R factor, the fit-quality reached with the $AlCo_3$ model is the same as that achieved for the MT model. Although the MT model might be ruled out by odd structural best-fit parameters and the evidence for double steps in the STM, LEED by its R-factor criterion alone cannot differentiate between the two models. This failure must be a consequence of the (too) many fit parameters involved in the MT model or, equivalently, a correspondingly too narrow data base width. Similarly, correlations between atomic vibrations and concentrations[61] make it hard to distinguish between the disordered $AlCo_3$ model and its fully ordered counterpart. Therefore, additional support for the $AlCo_3$ model is needed, and is provided by DFT calculations presented in the next two sections. We concentrate first on the structural predictions of DFT for the $AlCo_3$ model on the one hand, and for the Al- as well as the Co-terminated B2 model (making the MT model) on the other hand. Their comparison to the respective results obtained by LEED should allow one to identify the true structure. The energetics and stability of the phases are then considered in the final section.

VI. STRUCTURAL RESULTS BY DFT

In recent years, DFT has been shown to predict the structure of surfaces in excellent agreement with the results of experimental methods. Work by our own group has demonstrated such agreement for, e.g., H/Mo(111),[62] Br/Pt(110),[63,64] Ir(100)−(5×1)-hex,[65,66] FeSi/Si(111),[67] and CoAl(100).[6,38] So, one should be able to determine the structure of CoAl(111) unambiguously by computing the structure of the above $AlCo_3$ and MT models in DFT, and comparing them with the respective LEED results. The correct model should produce an exact match. Therefore, DFT

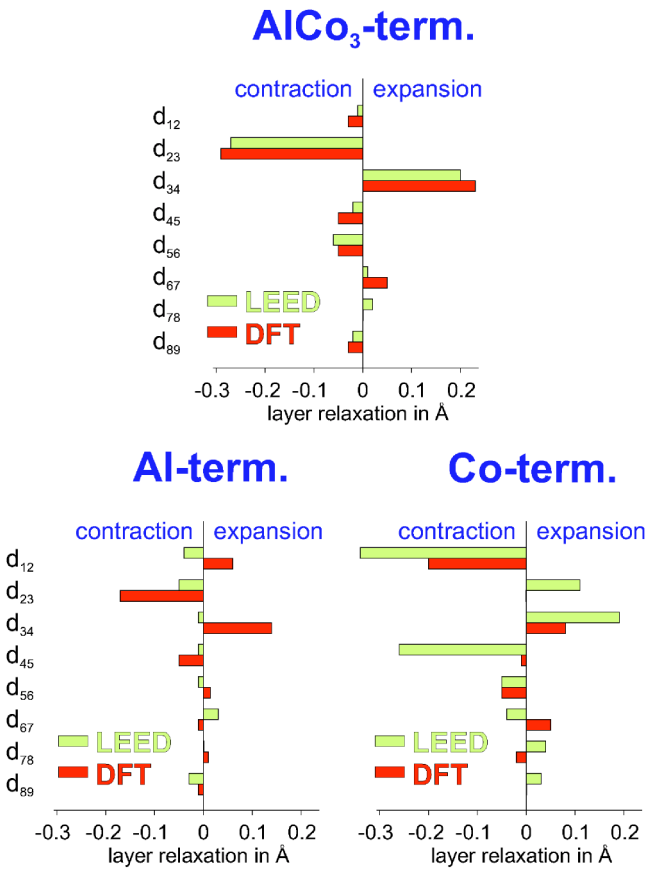

FIG. 5. (Color online) Comparison of the structural parameters derived from LEED and DFT for the structures given. Only for the $AlCo_3$-model LEED and DFT agree, proving this to be the correct structure.

calculations were carried out for the $AlCo_3$ model allowing for relaxations of the top eight layer spacings. The same was applied for the Al- and Co-terminated B2-phases which build the MT model. Table I compares the DFT results with those of LEED for the $AlCo_3$ model and Fig. 5 visualizes the comparison for both the $AlCo_3$ and the MT model.

As obvious from Fig. 5, DFT and LEED agree for the $AlCo_3$ model, with deviations never larger than 0.03 Å. In contrast, there are hardly any correlations between the LEED and DFT results for the Al- and Co-terminated B2 phases. The deviations reach up to 0.25 Å and even the sign of the relaxation is often at variance. This proves the $AlCo_3$ model to be correct and the MT model to be incorrect. As a consequence, the best fit parameters of the MT model in LEED have no physical relevance. While the $AlCo_3$ model is thus firmly established, it could still be kinetically stabilized. We will see in Sec. VII that it is also the energetically favored structure.

As a final point, we note that all bond lengths within the $AlCo_3$-model geometry appear physically sound. The nn distance between first layer Al atoms and second layer Co atoms is almost bulklike, while the nn distance to the fourth layer Co atoms is contracted by about 3%. Similar contractions are found for the bond lengths between second layer Co atoms and their nn in the third and fifth layers. Such reduced bond distances of "surface" atoms are quite common. In fact,

TABLE I. Structural parameter values for the MT model and the (ordered) $AlCo_3$ single-termination model resulting by DFT calculations. For the $AlCo_3$ model the values are compared to the LEED result with the statistical error limits given.

	$AlCo_3$ model		MT model	
			Al-term.	Co-term.
	LEED	DFT	DFT	DFT
Δd_{12}(Å)	−0.01±0.05	−0.03	+0.06	−0.20
Δd_{23}(Å)	−0.27±0.02	−0.29	−0.17	±0.00
Δd_{34}(Å)	+0.20±0.02	+0.23	+0.14	+0.08
Δd_{45}(Å)	−0.02±0.02	−0.05	−0.05	−0.01
Δd_{56}(Å)	−0.06±0.02	−0.05	+0.01	−0.05
Δd_{67}(Å)	+0.01±0.02	+0.05	−0.01	+0.05
Δd_{78}(Å)	+0.02±0.02	±0.00	+0.01	−0.02
Δd_{89}(Å)	−0.02±0.03	−0.03	−0.01	±0.0

they are comparatively small for a surface as open as CoAl(111). In contrast, the distances between third layer Co antisite atoms and the underlying Co atoms of the fourth and sixth layers are significantly expanded (4% and 5%, respectively). At a first glance, this expansion might be assigned to a special antisite relaxation effect, i.e., a mutual repulsion of atoms of the same type in an ordered AB alloy. While the DFT results for the bulklike Al-terminated surface reveal that just these distances are similarly expanded in case of a fully stoichiometrical B2 surface, there is a considerable lattice relaxation around the antisite atom otherwise. Comparing the computed relaxation profiles of the $AlCo_3$ model and the bulklike Al-terminated surface shows that the Co antisite atoms within the third layer are outward relaxed with respect to regular Al atom positions. This enhances the contraction and the expansion of second layer and third layer spacings, respectively, and reverses the (small) relaxation of the first layer spacing.

Beyond the confirmation of the $AlCo_3$ model as the model which corresponds to the experimentally prepared surface structure, the DFT calculations provide additional information. As previously stated in the introduction, and as proven in the next section, an exactly stoichiometric sample would exhibit an ideal Al-terminated surface of the B2-ordered crystal. For this case, our DFT calculations predict the detailed surface structure. The same holds for a Co-terminated surface, which cannot be excluded *a priori*.

VII. PHASE ENERGETICS AND PHASE STABILITY CALCULATED BY DFT

A. Mixed termination versus $AlCo_3$

One might expect that a few simple *ab initio* calculations of total energies could predict whether the $AlCo_3$ or the MT model is energetically favored. In fact, this direct statement would only be possible if the number of both Co and Al atoms were the same for each model, but this is not the case. We show below that the appearance of Co antisites within the CoAl(111) surface is only reasonable if such antisites

exist already in the material's bulk due to some slight off-stoichiometry, just as for CoAl(100).[6] In contrast, the *creation* of an antisite by atomic exchange processes in a stoichiometric bulk would be energetically very expensive (1.29 eV). At a temperature of about 800 K [at which the HT(1×1) phase develops], only a fraction of about 10^{-9} antisites would be thermally excited. For a 1 mm thick sample [$\approx 10^7$(111) layers] this would not be sufficient to form a single atomic layer of antisite defects—in contrast to a slight off-stoichiometry of, for instance, 10^{-3}.

The $AlCo_3$ and MT models do not share the same stoichiometry (an $AlCo_3$-capped surface contains more Co atoms). This induces a finite offset in the surface energies of each arrangement, which is rather drastic for the slab used in the DFT calculations [consisting of 19 (111) layers, see Sec. III), and independent of its thickness. Consequently, we cannot differentiate between the two models only on the basis of the total energies resulting from the DFT calculations. Yet we can consider the stability of those ordered structures using a thermodynamic description. In this thermodynamic model the surface's Gibbs function (surface formation energy per atom) is given by

$$\sum = \frac{1}{A_S}(G_S - N_{Al}\mu_{Al} - N_{Co}\mu_{Co}) \tag{1}$$

with the chemical potential of the elements μ_{Co} and μ_{Al} as variables. In a stable phase, this function is minimal, but the actual minimum structure now depends on the potentials μ_i. A_S is the number of surface atoms per unit cell and G_S is the free energy, which is approximated by the total energy from the DFT calculation, $G_S \approx E_{DFT}$. We can neglect the entropy contribution, as its vibrational part is small (<10 meV/atom at 1000 K).[68] Since we concentrate on ordered structures, the configurational contribution is also negligible. Assuming the surface to be in equilibrium with a certain bulk phase, we can write

$$x\mu_{Co} + (1-x)\mu_{Al} = g_b(x), \tag{2}$$

whereby g_b is the free energy per atom of the bulk phase, which consists of a B2 structure with antisites. This bulk free energy is also approximated by the total energies taken from the DFT calculations

$$g_b(x) \approx \tfrac{1}{2}E_{tot}(B2) + (x-0.5)E_{AS}(x), \tag{3}$$

whereby $\frac{1}{2}E_{tot}(B2)$ is the total energy of the ideal B2 phase per atom and $E_{AS}(x)$ is the antisite formation energy given by $E_{AS}(x)=[E_b(x)-E_b(\mathrm{B2})]/(x-0.5)$. Here, $E_b(x)$ is the total energy of a supercell containing $N\cdot(x-0.5)$ antisites. We may estimate $E_{AS}(x)$ in the limit of dilute bulk Co antisite defects, setting the Co concentration to 51.9%. For this value, $E_b(x)$ is calculated from the total energy of a single antisite in a 54 atom B2 cell, a cubic cell on the bcc lattice with a length of $3a$. The quantity $E_b(\mathrm{B2})$ is the total energy of an equally sized ideal B2 cell.

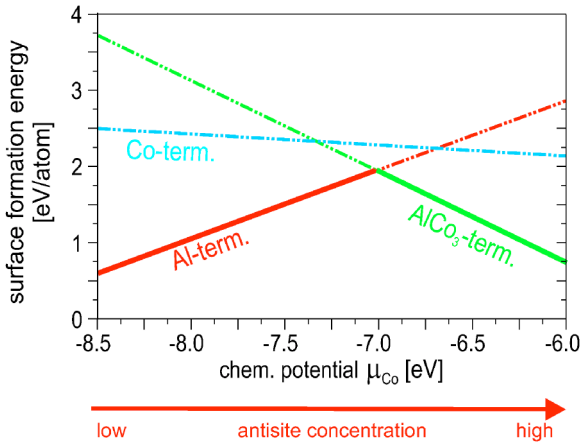

FIG. 6. (Color online) Stability diagram of the Co-, Al-, and $AlCo_3$-terminated B2 phases as function of the bulk stoichiometry controlled by the chemical potential of Co.

Assuming equilibrium between the surface and the bulk antisite reservoir and applying the appropriate stability conditions, we obtain an expression for the surface formation energy Σ which depends only on one of the chemical potentials (here, μ_{Co} is chosen):

$$\sum = \frac{1}{A_S}\left(E_{DFT} - N_{Co}\mu_{Co} - N_{Al}\frac{1}{1-x} \times \left[\frac{1}{2}E_{tot}(B2) + (x-0.5)E_{AS}(x)\right] - x\mu_{Co}\right). \tag{4}$$

Using Eq. (4), a stability diagram of different phases for the CoAl(111) can be constructed. This diagram is displayed in Fig. 6 for Al- and Co-terminated B2 ordered surfaces, and for the above $AlCo_3$ model. In order to allow the existence of the MT model, the formation energies for Co and Al terminations should not differ much more than by the thermal energy ($\approx$0.1 eV at $\approx$1200 K). Clearly, this criterion is only fulfilled in a region where the formation energy for the surface according to the $AlCo_3$ model is much lower, independent of the concentration or temperature values to which the abscissa corresponds. Therefore, the MT model is also excluded by energetic arguments, in addition to the comparison of LEED and DFT geometries in the preceding section.

B. Why Co antisites prefer the third layer, not the first

Before concluding, we illustrate (i) how antisite segregation in CoAl(111) is energetically favorable, and (ii) why it affects the third layer rather than the top layer. First, we calculate the energies, $E_s^{i,anti}$, of two atomic slabs with either the surface layer, $i=1$, or the third layer, $i=3$, consisting of Co antisites. This comparison settles the relative stability of both arrangements, but does not reveal whether either configuration is energetically favored over an Al-terminated B2-stacked slab without antisites. When comparing $E_s^{i,anti}$ with a purely B2-stacked slab, we are faced with the problem that this slab contains a different number of Co (Al) atoms, namely N_s^{Co} (N_s^{Al}) per unit cell, than the ($N_s^{Co}+2$) Co atoms

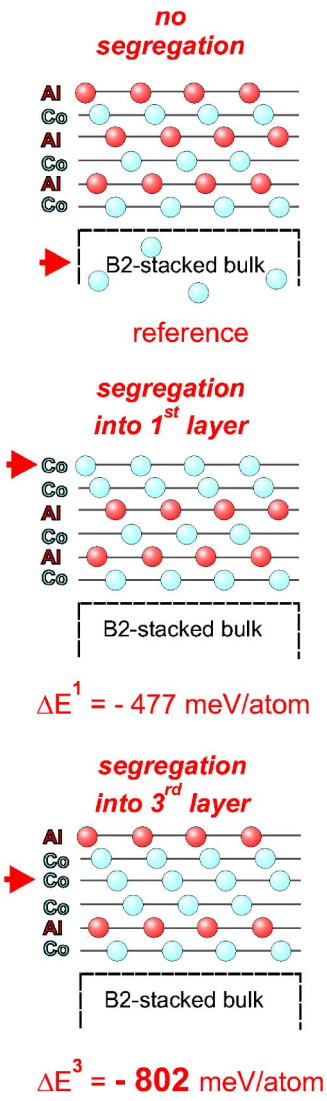

FIG. 7. Energetics for the segregation of Co antisites to the first and third Al layer of CoAl(111) (middle and bottom panel, respectively). The situation with all antisites accommodated in the bulk (top panel) serves as the energy reference.

and $(N_s^{Al}-2)$ Al atoms of the antisite slabs (note that each slab contains two surfaces). Therefore, we have to correct the energy of the B2-stacked slab by the energy difference between an ideally B2-ordered bulk crystal, E_b, and the energy of a B2-ordered bulk supercell which contains an antisite atom, E_b^{anti}. The relevant surface slab geometries are compared in Fig. 7, with the energy of the B2-stacked slab serving as the reference.

In total, we write the relevant energy difference as

$$\Delta E^i = [E_s^{i,anti} - E_s]/2 + E_b - E_b^{anti}, \qquad (5)$$

whereby $E_s = E_s(N_s^{Al}, N_s^{Co})$ is the energy of the undistorted surface slab, and $E_s^{i,anti} = E_s^i(N_s^{Al}-2, N_s^{Co}+2)$ is the slab energy with the *i*th layer of *both* slab surfaces replaced by antisite defects [the factor 1/2 in Eq. (5) accounts for the slab's two surfaces]. The quantity $E_b = E_b(N_b^{Al}, N_b^{Co})$ stands for the energy of a filled B2-stacked cell containing 54 atoms (i.e., without surfaces), and $E_b^{anti} = E_b(N_b^{Al}-1, N_b^{Co}+1)$ describes the same but with a Co antisite atom in the center.

In this scenario, the segregation energy of Co antisite defects to the topmost layer (i.e., forming a Co-Co-Al-Co-Al-Co…-stacking sequence) yields $\Delta E^1 = -477$ meV/atom. So, already this process is clearly energetically favorable. However, Co antisite defect segregation to the third layer (the $AlCo_3$ model) is even more favorable, $\Delta E^3 = -802$ meV/atom, as is shown in Fig. 7.

Handwavingly, these results can be explained by the competition between Al termination and the segregation of Co antisite defects, as described in the Introduction. In fact, the relatively open (111) surface benefits from both effects. In a simple nn-bonding picture, the surface compromises by rejecting the full energy gain which is associated with the segregation of Co antisites to the fourfold nn-undercoordinated topmost layer. By choosing the onefold undercoordinated third layer instead, the energy gain associated with three more bonds is lost, but the energetic advantage of placing Al at the outermost boundary of the crystal is retained. The overall energy gain is almost doubled by this "wise decision."

VIII. CONCLUSION

We have investigated the (111)-oriented surface of B2 transition-metal aluminide CoAl by AES, quantitative LEED, and DFT. Our unambiguous conclusion is that the surface is capped by an $AlCo_3$ sequence of (111) planes, and that the usual alternating stacking sequence of B2 follows only in deeper layers. Remarkably, this means that the surface stabilizes a full unit cell of the well-known bcc-based $D0_3$ structure, the A_3B superlattice of (111) atomic planes, although no such phase is reported in the Co-Al bulk phase diagram. Our findings cannot be explained as a property of the ideal stoichiometric B2 structure. Rather, they are a consequence of an inevitable slight Co excess of the near-surface region. Such an excess appears more the rule than the exception, since the stability range of bulk CoAl extends only into the Co-rich region of the phase diagram. Therefore, samples which are Al-rich in the bulk should not exist. In addition, conventional procedures of surface preparation (sputtering and annealing) always lead to an even further depletion of Al within the near-surface region. At best, an almost pure Al-termination might be found for rather virgin samples. Normal samples should show the behavior which was established in the present paper.

In a strongly bound material (CoAl, NiAl), off-stoichiometries must be incorporated as rather unfavorable structural defects—Co antisite defects in our case. These defects will accumulate near the surface to reduce unfavorable bonds. The tendency of aluminide surfaces to terminate with Al counteracts this effect, leading to the observed $AlCo_3$-like stacking sequence as an ideal compromise. The antisite segregation energy of about 800 meV is remarkably large. Therefore, even minuscule deviations from the ideal stoichiometry within the underlying "bulk" will be amplified at the surface by many orders of magnitude, which makes "proper annealing" utterly impossible.

Finally, we re-emphasize that our central result holds for strongly ordering compounds in general: a rather sharp switch of the segregation behavior must be expected whenever the stoichiometry line can be crossed, e.g., in the case of NiAl. Thus, a collection of seemingly similar samples which are only nominally stoichiometric may display very different segregation patterns. This is consistent with the somewhat varying results pertaining to NiAl(100) and NiAl(111). This caution with respect to the actual stoichiometry of a sample must be extended to other strongly ordering alloys. We expect more coherent behavior for well-defined off-stoichiometric materials than for their "fully" stoichiometric counterparts.

ACKNOWLEDGMENTS

The authors are indebted to Deutsche Forschungsgemeinschaft (DFG) for financial support. They also wish to thank G.R. Castro for providing the CoAl(111) sample.

*Present address: Abteilung Theorie, Fritz-Haber-Institut der Max-Planck-Gesellschaft, Faradayweg 4-6, 14195 Berlin-Dahlem, Germany.

[1] *Intermetallic Compounds*, edited by J. H. Westbrook (Wiley, New York, 1967).
[2] G. Tammann, Z. Anorg. Allg. Chem. **107**, 1 (1919).
[3] G. N. Derry, in *Handbook of Surfaces and Interfaces of Materials*, edited by H. S. Nalwa (Academic Press, San Diego, 2001), pp. 330–379.
[4] D. McLean, *Grain Boundaries in Metals* (Oxford University Press, London, 1957).
[5] M. Polak and L. Rubinovich, Surf. Sci. Rep. **38**, 127 (2000).
[6] V. Blum, L. Hammer, C. Schmidt, W. Meier, O. Wieckhorst, S. Müller, and K. Heinz, Phys. Rev. Lett. **89**, 266102 (2002).
[7] L. V. Pourovskii, A. V. Ruban, B. Johansson, and I. A. Abrikosov, Phys. Rev. Lett. **90**, 026105 (2003).
[8] J. Noonan and H. Davis, Phys. Rev. Lett. **59**, 1714 (1987).
[9] H. Niehus, Nucl. Instrum. Methods Phys. Res. B **33**, 876 (1988).
[10] S. Overbury, D. Mullins, and J. Wendelken, Surf. Sci. **236**, 122 (1990).
[11] R. Franchy, M. Wuttig, and H. Ibach, Surf. Sci. **189/190**, 438 (1987).
[12] J. F. Wendelken (private communication in Ref. 10).
[13] H. Niehus, W. Raunau, K. Besocke, R. Spitzl, and G. Comsa, Surf. Sci. **225**, L8 (1990).
[14] K. Heinz and L. Hammer, J. Phys.: Condens. Matter **11**, 8377 (1999).
[15] L. Hammer, W. Meier, V. Blum, and K. Heinz, J. Phys.: Condens. Matter **14**, 4145 (2002).
[16] H. Davis and J. Noonan, Mater. Res. Soc. Symp. Proc. **83**, 3 (1987).
[17] H. Davis and J. Noonan, in *The Structure of Surfaces II*, edited by J. F. van der Veen and M. A. Van Hove, Springer Series in Surface Science Vol. 11 (Springer, Berlin, 1988), pp. 152–159.
[18] D. Mullins and S. Overbury, Surf. Sci. **199**, 141 (1988).
[19] R.-P. Blum, D. Ahlbehrendt, and H. Niehus, Surf. Sci. **366**, 107 (1996).
[20] W. Roos, J. du Plessis, G. van Wyk, E. Taglauer, and S. Wolf, J. Vac. Sci. Technol. A **14**, 1648 (1996).
[21] E. Taglauer (private communication in Ref. 5).
[22] A. Stierle, V. Formoso, F. Comin, G. Schmitz, and R. Franchy, Physica B **283**, 208 (2003).
[23] H. Davis and J. Noonan, Phys. Rev. Lett. **54**, 566 (1985).
[24] H. Davis and J. Noonan, J. Vac. Sci. Technol. A **3**, 1507 (1985).
[25] M. Kang and E. Mele, Phys. Rev. B **36**, 7371 (1987).
[26] S. Yalisove and W. Graham, Surf. Sci. **183**, 556 (1987).
[27] A. Hanbicki, A. Baddorf, E. Plummer, B. Hammer, and M. Scheffler, Surf. Sci. **331–333**, 811 (1995).
[28] X. Torrelles, F. Wendler, O. Bikondoa, H. Isern, W. Moritz, and G. Castro, Surf. Sci. **487**, 97 (2001).
[29] W. Meier, V. Blum, L. Hammer, and K. Heinz, J. Phys.: Condens. Matter **13**, 1781 (2001).
[30] V. Blum, L. Hammer, W. Meier, K. Heinz, M. Schmid, E. Lundgren, and P. Varga, Surf. Sci. **474**, 81 (2001).
[31] M. Kottcke, H. Graupner, D. M. Zehner, L. Hammer, and K. Heinz, Phys. Rev. B **54**, R5275 (1996).
[32] H. Graupner, L. Hammer, K. Müller, and D. Zehner, Surf. Sci. **322**, 103 (1995).
[33] A. Baddorf and S. Chandavakar, Physica B **221**, 1413 (1996).
[34] L. Hammer, H. Graupner, V. Blum, K. Heinz, G. W. Ownby, and D. M. Zehner, Surf. Sci. **412–413**, 69 (1998).
[35] O. Kizilkaya, D. Hite, D. Zehner, and P. Sprunger, Surf. Sci. **529**, 223 (2003).
[36] L. Piccolo and L. Barbier, Surf. Sci. **505**, 271 (2002).
[37] V. Blum, C. Rath, G. R. Castro, M. Kottcke, L. Hammer, and K. Heinz, Surf. Rev. Lett. **3**, 1409 (1996b).
[38] O. Wieckhorst, S. Müller, L. Hammer, and K. Heinz, Phys. Rev. Lett. **92**, 195503 (2004).
[39] S. Müller, J. Phys.: Condens. Matter **15**, R1425 (2003).
[40] P. Nash and O. Kleppa, J. Alloys Compd. **321**, 228 (2001).
[41] R. Hultgren, P. Desai, D. Hawkins, M. Gleiser, and K. Kelly, in *Selected Values of the Thermodynamic Porperties of Binary Alloys* (Am. Soc. of Metals, Metals Park, OH, 1973).
[42] G. Bester, B. Meyer, and M. Fähnle, Phys. Rev. B **60**, 14 492 (1999).
[43] M. Kogachi and T. Tanahashi, Scr. Mater. **35**, 849 (1996).
[44] M. Hagen and M. Finnis, Philos. Mag. A **77**, 447 (1998).
[45] B. Meyer and M. Fähnle, Phys. Rev. B **59**, 6072 (1999).
[46] K. Heinz, Prog. Surf. Sci. **27**, 239 (1988).
[47] P. J. Rous, J. B. Pendry, D. k. Saldin, K. Heinz, K. Müller, and N. Bickel, Phys. Rev. Lett. **57**, 2951 (1986).
[48] P. Rous, Prog. Surf. Sci. **39**, 3 (1992).
[49] V. Blum and K. Heinz, Comput. Phys. Commun. **134**, 392 (2001).
[50] R. Döll, M. Kottcke, and K. Heinz, Phys. Rev. B **48**, 1973 (1993).
[51] K. Heinz, R. Döll, and M. Kottcke, Surf. Rev. Lett. **3**, 1651 (1996).
[52] A. Fox, J. Phys. F: Met. Phys. **13**, 1593 (1983).
[53] U. Löffler, R. Döll, K. Heinz, and J. B. Pendry, Surf. Sci. **301**,

346 (1994).
[54] M. Kottcke and K. Heinz, Surf. Sci. **376**, 352 (1997).
[55] J. Pendry, J. Phys. C **13**, 937 (1980).
[56] J. Perdew and Y. Wang, Phys. Rev. B **45**, 13 244 (1992).
[57] G. Kresse and J. Furthmüller, Comput. Mater. Sci. **6**, 15 (1996).
[58] P. Mrozek, M. Meynhard, J. Wernisch, and A. Jablonski, Phys. Status Solidi A **84**, 39 (1984).
[59] M. Wiets and M. Weinelt (private communication).
[60] R. Baudoing, Y. Gauthier, M. Lundberg, and J. Rundgren, J. Phys. C **19**, 2825 (1986).
[61] V. Blum, L. Hammer, W. Meier, and K. Heinz, Surf. Sci. **488**, 219 (2001).
[62] M. Arnold, A. Fahmi, W. Frie, L. Hammer, and K. Heinz, J. Phys.: Condens. Matter **11**, 1873 (1999).
[63] V. Blum, L. Hammer, K. Heinz, C. Franchini, J. Redinger, K. Swamy, C. Deisl, and E. Bertel, Phys. Rev. B **65**, 165408 (2002).
[64] C. Deisl, K. Swamy, N. Memmel, E. Bertel, C. Franchini, G. Schneider, J. Redinger, S. Walter, L. Hammer, and K. Heinz, Phys. Rev. B **69**, 195405 (2004).
[65] D. Spišsák and J. Hafner, Surf. Sci. **546**, 27 (2003).
[66] D. Lerch, Master's thesis, Universität Erlangen-Nürnberg, 2004.
[67] S. Walter, R. Bandorf, W. Weiß, K. Heinz, U. Starke, M. Strass, M. Bockstedte, and O. Pankratov, Phys. Rev. B **67**, 085413 (2003).
[68] K. Reuter and M. Scheffler, Phys. Rev. B **65**, 035406 (2002).